13 Martian Atmospheric Evolution: Implications of an Ancient Intrinsic Magnetic Field

Helmut Lammer, Willibald Stumptner and Gregorio J. Molina-Cuberos

The Magnetometer / Electron Reflectometer (MAG/ER) experiment on board of Mars Global Surveyor (MGS) has detected surface magnetic anomalies of up to 1500 nT during its low aerobreaking passes, resulting from remnant crustal magnetism. These magnetic anomalies strongly indicate the existence of a strong ancient intrinsic Martian magnetic moment, which corresponded to a magnetic field strength of 10% - 100% of present Earth's.

Such an ancient intrinsic magnetic field had significant consequences for the evolution of the Martian atmosphere, especially by reducing the amount of certain atmospheric constituents lost to space. The evolution of the Martian atmosphere, with regard to water, is influenced by non-thermal atmospheric loss processes of heavy atmospheric constituents. Since Mars does not have an appreciable intrinsic magnetic field at present and a comparatively small gravitational acceleration, all known atmospheric loss processes work and several important atmospheric constituents, namely H, H_2, N, O, C, CO, O_2 and CO_2 are lost from the atmosphere. The escape rates of atmospheric constituents over time, including the loss of H_2O from Mars indicate that the red planet could have lost an atmosphere of at least 1 bar to space during the past 3.5 billion years.

The second important effect of an ancient intrinsic magnetic field and a much denser atmosphere is the shielding of the Martian surface from cosmic rays and UV radiation. Cosmic rays - which consists of charged particles - are deflected by the magnetic field depending on their energy and only high energy particles are able to penetrate and reach the surface. UV radiation is partially absorbed in planetary atmospheres, as is discussed in detail in Chaps. 14, Cockell; and 15, Rettberg and Rothschild. By investigating the surface protection during the history of the Martian atmosphere one can see that the atmospheric conditions on Mars were comparable to Earth, 3.7 billion years in the past. As life on Earth may be as old as 3.8 billion years, similar life forms may have developed on early Mars under those more favorable atmospheric conditions.

13.1 Nonthermal Atmospheric Escape Processes

Atmospheric escape occurs when atoms move upward with velocities greater than the escape velocity to an atmospheric level, where the collision probability is low (i.e. the

critical level or exobase) [1]. Nearly all of the non-thermal atmospheric escape mechanisms involve ions. Many of them, such as charge exchange, dissociative recombination and sputtering processes in planetary atmospheres release energies, which appear in the form of excitation and kinetic motion of neutral products. The kinetic energies of these newly born hot atoms in some cases are in the order of electron volts. The escape fractions of a hot oxygen atom released by various non-thermal escape processes is calculated with a *Monte Carlo* technique. The hot oxygen atoms produced are assumed to become thermalized eventually by a series of elastic hard sphere collisions with the colder background gas such as CO_2, O_2 or O. Inelastic collisions are negligibly small at these low energies. On Mars all oxygen atoms at the exobase with energies greater than 2 eV are able to escape. After its release, a hot oxygen atom may collide with the neutral background gas, may change its direction, lose its energy or the atom may travel long distances in the atmosphere without collisions [2-4]. If the starting altitude is close to the exobase or above, then the escape fraction is about 1, corresponding to atmospheric levels, where the collision probability is low and thus all atoms with energies greater than the escape energy can actually escape. In Table 13.1. we have summarized exobase altitudes h_{ex} and temperatures T_{ex} (which vary with the Suns' activity cycle), escape velocities v_∞ and escape energies E for O, N and CO_2 for Venus, Earth and Mars.

13.1.1 Charge Exchange and Dissociative Recombination

Thermal ions in planetary ionospheres can be converted to fast neutral atoms with ballistic trajectories reaching very high altitudes via charge exchange interaction with neutral atomic hydrogen and oxygen (see Eqs 13.1 and 13.2).

Both reactions have been invoked to explain the existence of an extra component of suprathermal hydrogen in the exosphere of Venus [5-10]. A more important mechanism for the production of hot atomic oxygen in the Martian exosphere is the dissociative recombination of ionospheric O_2^+ ions.

Table 13.1. A summary of average exobase altitudes h_{ex} and temperatures T_{ex}, escape velocities v_∞ and escape energies E for O, N and CO_2 for the most important terrestrial planets

	h_{ex} [km]	T_{ex} [K]	v_∞ [km/s]	E_O [eV]	E_{CO2} [eV]	E_N [eV]
Venus	≈ 200	≈ 600	10.40	8.96	24.64	7.84
Earth	≈ 300	≈ 1000	11.20	10.40	28.60	9.10
Mars	≈ 200	≈ 220	5.02	2.08	5.72	1.82

$$O^+ + H \rightarrow O(hot) + H^+ \tag{13.1}$$

$$O^+ + O \rightarrow O(hot) + O^+ \tag{13.2}$$

Dissociative recombination is a photochemical process that can impart sufficient energy (about 0.125 eV/amu) to the produced atoms so they can escape Mars' gravitational field. Mostly N in the form of N_2^+, O as O_2^+ and C as CO^+, all of them Martian atmospheric constituents, are affected and the resulting neutral escape flux can be modeled. However, oxygen is by far the most important constituent for dissociative recombination on Mars. This requires knowledge of the density and composition of the Martian ionosphere and atmosphere. To understand the formation of the hot oxygen atoms [11-13], we investigate four possible channels. The oxygen atoms may be formed in the ^3P, ^1S and ^1D states, which correspond to excited oxygen atoms (one electron in a higher energetic state) with varying amounts of kinetic energy (in eV, see Eqs. 13.3 to 13.6). The upper left index means that the energy level of the exited atom belongs to a system of single-, double-, triple-, etc. levels. The letter S, P, D, etc. denotes a group of levels within this system e.g., ^3P is a triplet P level.

$$O_2^+ + e \rightarrow O\left(^3P\right) + O\left(^3P\right) + 6.96eV \tag{13.3}$$

$$O_2^+ + e \rightarrow O\left(^3P\right) + O\left(^1D\right) + 5.00eV \tag{13.4}$$

$$O_2^+ + e \rightarrow O\left(^1D\right) + O\left(^1D\right) + 3.02eV \tag{13.5}$$

$$O_2^+ + e \rightarrow O\left(^1D\right) + O\left(^1S\right) + 0.8eV \tag{13.6}$$

The branching ratios for dissociative recombination of oxygen atoms were measured for the final channels [4]: O(^{3}P) + O(^{3}P) : O(^{3}P) + O(^{1}D) : O(^{1}D) + O(^{1}D) : O(^{1}D) + O(^{1}S) = 0.22 : 0.42 : 0.31 : 0.05. The escape flux Φ_{esc} is obtained by integrating the energy spectrum of the cumulative hot oxygen atom flux $F(E,z_e)$ at the exobase as a function of the kinetic energy E in the energy interval between the escape energy E_{esc} and the maximum energy E_{max}.

$$f_{esc} = \int_{E_{esc}}^{E_{max}} F\left(E, z_e\right) dE \tag{13.7}$$

The escape flux for hot oxygen atoms originating from dissociative recombination (*exospheric O*) for Mars is at present about 6×10^6 cm^{-2}s^{-1} corresponding to an escape rate of 6×10^{24} s^{-1} [14, 15]. A direct result of dissociative recombination is the formation of a hot oxygen *corona* around Mars [16, 17]. Such a corona consists of atmospheric particles moving on ballistic trajectories, since their energies are higher than the energy of the background gas, but lower than the escape energy. These corona particles interact with the solar-wind and, therefore, are a source for several other escape processes like atmospheric sputtering using coronal oxygen atoms ionized by the solar-wind as sputtering agents. The solar-wind is the flux of energetic charged particles ejected by the Sun into the interplanetary medium, mainly H^+ and He^+. It has an eroding effect on atmospheres of solar system bodies which are not shielded by strong intrinsic magnetic fields.

The escape flux for the dissociative recombination of CO^+ was estimated to be at least one magnitude less than the oxygen escape [18]. Substantial quantities of nitrogen atoms have escaped from Mars through electron dissociative recombination, producing hot nitrogen atoms with energies exceeding the escape energy for ^{14}N isotopes via intermediary N_2^+ and NO^+ ions [19].

Support for this escape hypothesis was provided by the Viking mass spectrometer, which recorded an anomalous $^{15}N/^{14}N$ ratio. Only $N(^4S)$ and $N(^2D)$ have enough energy to escape. More ^{14}N can escape from the planet than the heavier ^{15}N isotope. The escape rate of nitrogen from Mars is to be an estimated 2.3×10^5 s^{-1} for low and 8.9×10^5 s^{-1} for high solar activity [20], as the later corresponds to higher ionospheric production rates of nitrogen ions and, therefore, an increased escape.

13.1.2 Atmospheric Sputtering

The yield for atmospheric sputtering processes Y is defined as the number of species ejected per ion incident on an exobase of a gravitationally bound gas (which is on Mars mostly O and CO_2). It includes particles ejected as a result of a direct collision with the ion and those ejected due to a cascade of collisions initiated by the ions [21]. The escape yield Y for the principal atmospheric constituent near the exobase is:

$$Y = \frac{0.5\sigma_{T\geq U}}{cos\theta\sigma_d} + \frac{3S_n\alpha}{\pi^2 U\sigma_d} \tag{13.8}$$

with θ the entry pitch angle of the incident particle, T the particle energy, U the escape energy of the particle at the exobase, σ the collision cross-section for a particle receiving an energy transfer $T > U$ and σ_d the cross section for escape of a struck particle. The constants $3/\pi^2$ and α are obtained from the transport equation and S_n is the stopping cross-section [22]. Both the extreme ultraviolet (EUV) flux and the parameters of the solar-wind influence the flux of the sputtered particles. Mostly CO_2 and O are lost after being hit by reentered O^+ ions. These O^+ ions of exospheric origin are accelerated by the interaction of the solar-wind and interplanetary magnetic field (IMF) with the upper atmosphere. These ions follow helical trajectories along the interplanetary magnetic field lines draped over Mars and often re-impact the atmosphere with significant amounts of energy (upwards of 1 keV).

During the impact they can - through collisions - accelerate other particles, causing some of them to escape the planet. Most estimates do not take into account the expansion of the exosphere due to the heating caused by the ion impacts, so they may be viewed as lower limits.

There has been much debate recently about the sputtering efficiency (the number of particles ejected per incident particle) and dissociation cross section for an collision between O^+ and CO_2 [23-27]. Depending on the value chosen one gets different results in the calculation of escape rates for ancient Mars. The escape rates of sputtered O atoms from Mars are estimated at present to be about 3.0×10^{23} to 1.6×10^{24} s^{-1} and 8.0×10^{23} s^{-1} for CO_2 molecules [25].

13.1.3 Solar-Wind Interaction Processes

The massive plasma escape through the magneto-tail region on Mars, which was detected from the plasma instruments aboard the Phobos 2 spacecraft, could also be explained on the basis of ion-momentum considerations [28], since Mars at present has a negligible small intrinsic magnetic field.

A strong intrinsic magnetic field would protect the planet from most of the eroding effect of the solar-wind on the upper Martian atmosphere. Without such shielding, the solar-wind transfers momentum to atoms and ions on high ballistic trajectories and they can be swept away from the planet by the solar-wind. In Fig. 13.1 we have depicted O^+ ions following helical trajectories along magnetic field lines away from the planet.

During the Phobos 2 mission a maximum possible escape rate of about 2×10^{26} s^{-1} has been estimated if all the escaping particles are assumed to be O_2^+ ions. It is suggested that the O_2^+ ions observed from Phobos 2 owe their origin to the solar-wind erosion process in the Martian dayside ionosphere [29]. The effects of such an erosion

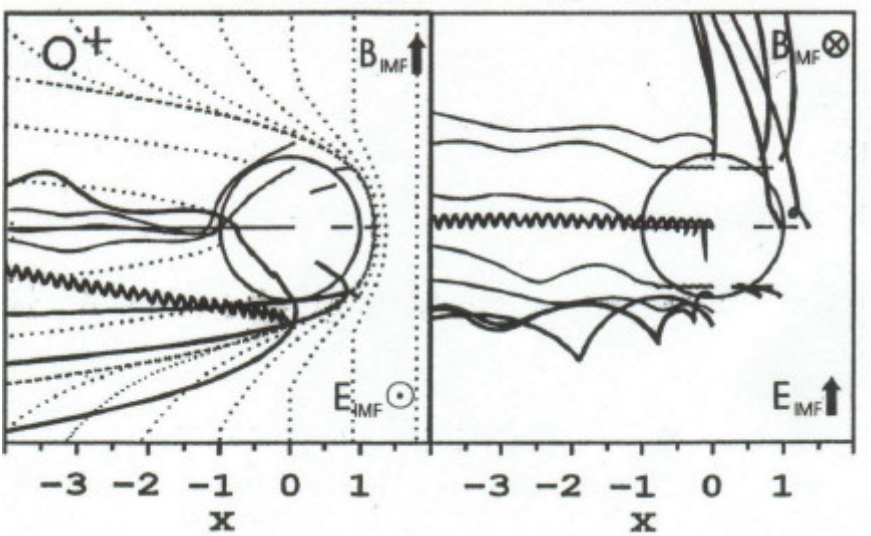

Fig. 13.1 Oxygen ions escaping Mars along interplanetary magnetic field lines on helical trajectories. BIMF and EIMF are the interplanetary magnetic and electric field. One can also see that some oxygen ions re-impact the atmosphere and act as sputtering agents.

process extend down to photochemical altitudes in the ionosphere of Mars. The estimated theoretical maximum ion escape rates from this erosion, by using Viking ionospheric data for the model, are in the range of $3\text{-}4\times10^{26}$ ions s^{-1}. As can be seen in Table 13.2., this is the most significant atmospheric escape process at present. However, during Mars' history other non-thermal escape processes e.g., sputtering have dominated.

13.1.4 Ionospheric Bubbles

A Kelvin-Helmholtz instability may cause the formation of ionospheric bubbles [30]. This instability occurs when two fluids are moving relative to each other and the boundary between them becomes unstable. This leads to a disturbance, which manifests as a travelling plasma wave in the case of Mars. This wave-like fluctuation in pressure, density and temperature grows in amplitude as long as the energy necessary to set up and maintain the instability is provided from the incoming plasma stream, i.e. the solar-wind.

The instability causes an exchange of momentum between two velocity layers, from the solar-wind plasma flow to the travelling wave to maintain its own motion. A break-up of the ionopause and the formation of a ionospheric bubble can result from these instabilities. Such an ionospheric bubble originates when a current tube is formed and ionospheric plasma is trapped in the boundary layer flow just upstream of the ionopause. The strong shear flows in this region should break up this structure and the ionospheric plasma is transported into the downstream tail region of the planet.

The formation of ionospheric bubbles happens only during a time of increased solar-wind velocity vSW (600 km/s $\leq$ vSW $\leq$ 800 km/s). About 100 bubbles can be formed during one ionopause break-up, causing a loss of approximately 5×10^{24} O_2^+ ions per bubble [31]. The ASPERA ion composition experiment [32] on board of Phobos 2 has detected such an ionospheric outflow and confirmed the estimated magnitude of atmospheric loss (O_2^+, O^+ etc.), with the exception of CO_2^+ ions, where the loss cannot be explained by ionospheric bubbles, as the concentration of CO_2^+ ions near the ionopause is negligible.

All the escape rates for oxygen, nitrogen and CO_2 discussed here are summarized in Table 13.2. for easy reference.

Table 13.2 Summary of model escape rates for oxygen, nitrogen and CO_2 for Mars at present.

Loss process	Model escape rates [s^{-1}]	Reference
Sputtered O	1.6×10^{24}	[26]
Sputtered CO_2	8.0×10^{23}	[26]
Exospheric O	5.0×10^{24}	[19]
Exospheric N	$2.0 - 9.0\times10^{5}$	[18]
Pick up O	6.0×10^{24}	[23]
Field line transport O_2^+	1.5×10^{23}	[43]
Field line transport CO_2^+	5.0×10^{22}	[43]
Ionospheric bubbles O_2^+	5.0×10^{24} / event	[31]
Erosion effect O_2^+	$3.0 - 4.0\times10^{26}$ / event	[29]

13.2 The Early Dense Martian Atmosphere

The present thin Martian atmosphere with a surface pressure of about 7 mbar has been one of the great puzzles in our solar system. Ancient fluvial networks on the surface of Mars suggest that it was warmer and wetter three billion years ago. Surface features resembling massive outflow channels provide evidence that the Martian crust contained the equivalent of a planet wide reservoir of H_2O several hundred meters deep [33, 34]. There are two possibilities for the fate of early H_2O and CO_2 - they are either sequestered somewhere on the planet or have been lost to space.

Impact erosion [35, 36] and late impact accretion [37, 38] are other processes which could have played an important role in affecting the early Martian atmosphere. Because both the Sun [39] and the Martian atmosphere have changed over time, the importance of these evolutionary processes cannot be estimated by simply multiplying the contemporary loss rates by the age of the solar system. Models of these loss mechanisms must include the evolution of solar EUV intensity, solar-wind effects and the ancient intrinsic magnetic field barrier.

13.2.1 The Quest for Water

Calculating sputtering rates of CO_2 molecules by re-entered O^+ pick up ions for 1 EUV (present), 3 EUV (3 times present EUV intensity, 2.5 Ga ago) and 6 EUV (6 times present EUV intensity, 3.5 Ga ago) epochs of the Martian atmosphere one finds an integrated CO_2 loss equivalent to about 0.14 bar to 3 bar. Integrating the atmospheric loss rates mentioned above of O and CO_2 backward in time one gets a much denser atmosphere in the past.

Figure 13.2 shows that the early Martian atmosphere had a total surface pressure from at least 1 bar up to 5 bars, depending on the atmospheric loss models used in the study (solid line [23]; dotted line [26]). Several studies used the calculated oxygen loss rates for the estimation that Mars has lost to space an equivalent depth of 50 meters of H_2O over the last 3.5 billion years [23, 26].

A recent study [27] used a 3-dimensional (3D) Monte-Carlo model to describe the sputter interaction of the incident pick up ions with the Martian atmosphere. In this detailed analysis the extrapolated loss by sputtered O atoms from the decay of the early Mars magnetic field ($\approx$ 3.7 Ga ago) to present time suggests lower escape rates.

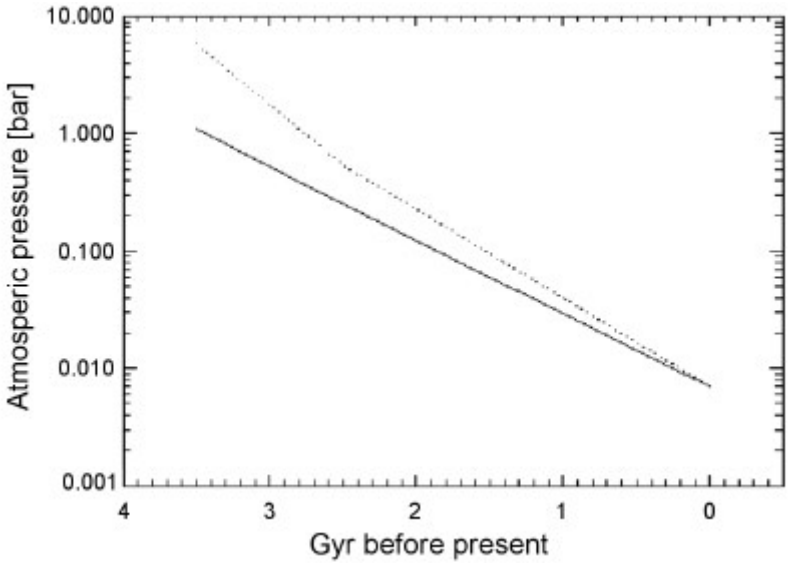

Fig. 13.2. Historical development of the Martian surface pressure. The dotted line is based on extremely high atmospheric sputtering rates [26], and the solid line on more moderate atmospheric sputtering rates [23].

In contrast to these studies we used the hydrogen loss as limiting factor for the loss of water from Mars [14], since for the early Martian atmosphere with its higher exospheric temperatures, where limiting flux conditions are likely to occur, the control of hydrogen escape by non-thermal O escape will not operate [40].

The results shown in Fig. 13.2 imply a maximum loss of H_2O to space equivalent to a depth less than 10 meters over the past 3.5 billion years. This amount is significantly lower than the early estimations, which use the non-thermal O escape rates as a limiting factor for the loss of water but is in good agreement with works based on the analysis of the D/H ratio in the Martian atmosphere [14] and in the Zagami SNC meteorite which is supposed to be of Martian origin [41]. Both isotope studies suggest that about 4 meters of H_2O were lost to space over the period considered by us, leaving today still a reservoir of crustal water, although it has been argued that the bulk of the water escape (hundreds of meters) must have happened in the first 0.5-1 Ga.

If we compare our results with the geological estimates of H_2O on Mars [33, 34] there still should be several tens of meters of water left in the form of ice and permafrost.

13.3 The Intrinsic Martian Magnetic Field

We have shown that loss of atmospheric species to space has played an important role in the evolution of the Martian atmosphere. The detection of surface magnetic anoma-

lies by MGS, which imply the existence of an intrinsic magnetic field may have consequences for various non-thermal escape mechanisms to space in the past. Calculations by using early solar ionizing flux and solar-wind models suggest that atmospheric sputtering was more important in the past. An ancient intrinsic magnetic field can protect against the sputtering and solar-wind induced loss in several ways.

The intrinsic magnetic field deflects the solar-wind around the atmosphere by eliminating solar-wind induced ionization processes and shields ions produced in the upper atmosphere from the solar-wind. Therefore, losses of atmospheric ions and atoms by pick up or collisional sputtering are minimized during Earth-like magnetic field periods. A strong intrinsic magnetic field would be a barrier for atmospheric sputtering processes. Only loss of neutral O and N atoms originating from dissociative recombination and upward flowing ionospheric CO_2^+ and O_2^+ ions over the Martian polar caps of the magnetosphere would be important [42, 43].

Planetary intrinsic magnetic fields are generated by electrical currents circulating through the molten mantle and core of a planet. It can be explained as a magnetic dipole located in the planetary center, with elements of higher order as additional contributors. The dipole moment of Earth M_{Earth} is about 8×10^{25} Gauss cm^3. The absolute value of the magnetic field H can be calculated at a magnetic latitude ϑ and distance r with:

$$H = \frac{M}{r^3}\sqrt{1+3\sin^2 J} \tag{13.9}$$

This corresponds to a H ≈ 0,3 Gauss ≈ 30 000 nT at the Earth's equator (and twice that at the poles) with typical variations of the order of tens of nT.

The MAG/ER instrument on the MGS spacecraft has obtained magnetic field and plasma observations throughout the near Mars environment, from beyond the influence of Mars to just above the surface at an altitude of about 100 km. Measurements made early in the mission established that Mars does not currently possess a significant intrinsic global magnetic field, with estimated upper limits for the magnetic moment of 2×10^{21} Gauss cm^3 [44] or surface magnetic fields less than 5 nT.

During the same time the detection of strong, small scale crustal magnetic anomalies associated with the ancient, heavily cratered terrain revealed that Mars must have had an internal active dynamo in its past, which is extinct at present. The most intense magnetic crustal sources lie in the Terra Sirenum region where measured total field intensities at around 100 km altitude exceed 1500 nT [45].

The crustal magnetic anomalies in this area are sufficiently high that the magnetic fields in and above the ionosphere locally increase the total pressure that stands off and deflects the solar-wind at Mars, resulting in an asymmetric bow shock when this region rotates through the sunlit side of the planet. This configuration results in the formation of multiple small magnetospheric cusps and magnetic reconnection regions with the interplanetary magnetic field.

13.3.1 The Ancient Martian Magnetosphere: Constraints for Atmospheric Escape

One can assume two different models of core formation for Mars [46, 47]. In the first model, a solid inner core develops at approximately 1.3 Ga, which adds heat and subsequently renews the strength of the magnetic field up to present. The first measurements of MGS almost certainly ruled out this scenario. The second model is a liquid core model where postaccretionary heat drives vigorous thermal convection within the core and sustains a planetary magnetic field. The initial dynamo field can be estimated from thermal evolution models [46]. By assigning a field generating current to a toroid with a radius $(r_c+r_{ic})/2$ and a cross-sectional radius $(r_c-r_{ic})/2$, with r_c the core and r_{ic} the inner core radius, the magnetic dipole moment of Mars normalized to Earth's can be calculated from [46, 47]:

$$\frac{M_{Mars}}{M_{Earth}} = 10^9 (r_c - r_{ic}) \sqrt{P_d} (r_c + r_{ic})^{\frac{3}{2}} \tag{13.10}$$

where P_d is the power associated with ohmic dissipation in the liquid outer core [48]. The majority of the crustal magnetic sources detected by MGS lie in an ancient, densely cratered terrain of the Martian highlands, south of the crustal dichotomy boundary [46]. This dichotomy boundary is the geologic division between the heavily cratered highlands to the south and the relatively young, smooth plains to the north where the Martian crust is thinner.

No magnetic anomalies were detected in the major Martian volcanic areas. The large impacts that formed the Hellas and Argyre basins and that are believed to have formed about 4 Ga ago are also not associated with magnetic crustal anomalies. The absence of crustal magnetic fields in these areas implies that the Martian dynamo had already ceased to operate when these impact basins were formed. This evidence supports the magnetic field models of a hot early Mars immediately after accretion followed by rapid cooling and crust formation [46, 47].

The concentration of a light constituent like sulfur in a mainly iron core is essential for the temporal evolution of the dynamo. During the cooling process of the core, the pure iron freezes out to form a solid inner core. The boundary layer between the inner and the outer core is enriched in the light constituent, leading to gravitational instability and upward flow driving the dynamo. Model calculations show that no inner core freeze-out occurs during the first 4.5 Ga if a sulfur content >15% is assumed. If the sulfur content is much lower than 15%, a solid inner core is formed that grows rapidly on a geologic time scale once it begins to freeze out. The lack of a present intrinsic magnetic field suggests that the core has either largely frozen out or never formed. The dipole moments calculated with a sulfur content estimated from SNC meteorites (≈15%) in the core are consistent with no inner core freeze-out. Rapid initial cooling of the whole planet leads to a decreased thermal convection in the core, until the Curie point is reached and the dynamo action ceases. Calculations depending on the sulfur content, P_d and core radii yield magnetic dipole moments of Mars normalized to Earth's of about 0.1 to 1.0, 3.7 Ga ago [45-48].

The first 500 to 700 million years after Mars was formed in the solar nebular its planetary magnetic field protected the atmosphere against loss by atmospheric sputter-

ing and solar-wind interaction processes. The deflection of the solar-wind around the bulk of the atmosphere by a magnetic field limits the ion production rate in the upper atmosphere by eliminating solar-wind induced ionization processes. More important, the field shields any ions produced in the upper atmosphere (e.g., by photo-ionization) from the solar-wind magnetic field. Therefore, losses of atmospheric ions and atoms by direct sweeping or collisional sputtering, respectively, are minimized. It was found that even a small magnetosphere can significantly decrease the ion production rate by a factor of about 2 orders of magnitude [49].

One can conclude from the MAG/ER results of the MGS mission that the Martian atmosphere was unprotected by its magnetosphere since 3.5 Ga ago. After this period the non-thermal escape processes removed most of the atmosphere (see Fig. 13.2).

13.4 Shielding of Hypothetical Primitive Martian Life Forms from Energetic Cosmic Particles and Radiation

The hunt for life on Mars was reanimated after the investigation of the 1.9 kg meteorite, ALH84001. The meteorite dates from about 4.5 Ga ago, formed early in Mars' history at a depth of a few kilometers. Impacts cracked and fractured ALH84001. 3.6 Ga ago groundwater seeped through fissures and filled them with carbonate mineral. About 16 million years ago an asteroid struck the Martian surface and ejected material, including ALH84001 to escape the gravitational pull. The Martian meteorite fell to Antarctica 13 000 years ago. Three types of evidence found in the carbonate filled fractures of the meteorite back the claim for early Martian live forms: (1) Organic molecules like such produced by breakdown and geologic aging of fossilized organic matter. (2) Pancake-shaped globules, made up of minerals that on Earth can be formed by bacteria. (3) Jellybean shaped and threadlike bodies that resemble fossil microbes [50, 51].

Although there are critical arguments too [e.g., 52], the notion of life existing on Mars, now or in the past, is not implausible since the planet is like a smaller version of Earth and its atmospheric and magnetospheric conditions seem to have been similar until about 3.5 Ga ago. One of the critical issues in the discussion of environmental conditions on early Mars is its radiation environment. We discuss this in more detail in the following paragraph.

13.4.1 Cosmic Ray Particle Fluxes on the Surface of Ancient Mars

Galactic cosmic rays are isotropic radiation produced outside our solar system. They consist mainly of protons 93% and α-particles 7%, with a minor component of heavier nuclei, < 0.7 %. The integral spectrum of cosmic ray particles follows a power law dependence on kinetic energy $E^{-1.74\pm0.1}$ [53]. The main mechanisms affecting the galactic cosmic ray propagation through the solar system are deceleration by the solar-wind in the interplanetary medium and deflection by magnetic fields near the Sun or planets.

The particle flux in an atmosphere arises from the rupture of α-particles forming primary cosmic rays and from the impact of high-energy protons and neutrons on the

atmospheric molecules. In such a collision other particles, such as protons and pions, are also produced:

$$\{p,n\}+N_2 \rightarrow n_p p + n_p n + n_{p^\pm} p^\pm + n_{p^0} p^0 \tag{13.11}$$
$$p^\pm \rightarrow m^\pm + neutrino$$
$$p^0 \rightarrow 2\,g$$
$$m^\pm \rightarrow e^\pm + 2\ neutrinos$$

where ν_i is the number of *i*-type particles resulting from the collision of a nucleon with a nucleus. The interaction of pions with the atmosphere is very complex. Charged and neutral pions decay to muons and gamma rays, respectively. Gamma rays interact with the atmosphere through the electromagnetic cascade production of electron-positron pairs, Bremsstrahlung and Compton process. Muons decay into two neutrinos and a fermion.

The atmospheric flux of the cosmic ray induced particles on the surface of ancient Mars is obtained by solving the Boltzmann equations governing the propagation of protons, neutrons, muons and pions in a 1 bar atmosphere, corresponding to more moderate non-thermal atmospheric loss rates [23]. The particle fluxes are calculated by using the same algorithm and codes [54] already used to predict the ion production rate in the atmosphere of Saturn's moon Titan [55]. Figure 13.3 shows the cosmic ray particle flux on the Martian surface 3.5 Ga ago, assuming an atmospheric pressure of about 1 bar. We neglected the magnetic field influence since it is assumed that the intrinsic Martian magnetic field vanished 3.7 Ga ago [45].

Before 3.7 Ga the ancient magnetosphere produced a radiation belt akin to the Van Allen belts of Earth, with a similar protecting effect against high energetic charged particles. Such a radiation belt reduces the flux of cosmic ray particles in the energy range of several MeV to several hundred MeV by a factor of:

$$\frac{j}{j_0} = e^{-\frac{E}{E_0}} \tag{13.12}$$

with E being the particle energy, E_0 being an energetic constant over a broad energy range, j the energy spectrum of the energetic particles in the radiation belt and j_0 being the energy spectrum of cosmic radiation in interplanetary space [56]. Only cosmic rays at the lower end of the considered energy spectrum (~10 MeV) are significantly affected by the magnetic field and the radiation belt it produced. The shielding effect of a dense early atmosphere by far dominates over the contribution of the early stronger magnetic field [57]. For comparison with the ancient Martian conditions, Fig. 13.4 shows the cosmic ray particle flux at present. Today Mars is only protected by its thin 6 mbar CO_2 atmosphere. Most of the particles reach the unprotected surface and the flux is, therefore, several orders of magnitude larger.

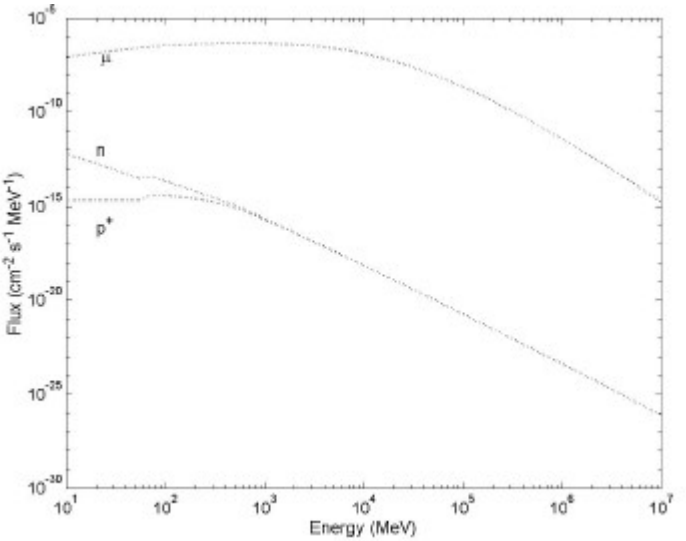

Fig. 13.3 Flux of cosmic ray particles at the surface of ancient Mars, 3.5 Ga ago shortly after the intrinsic Martian magnetic field vanished. The atmospheric pressure at this time is about 1 bar corresponding to more moderate non-thermal loss rates [23].

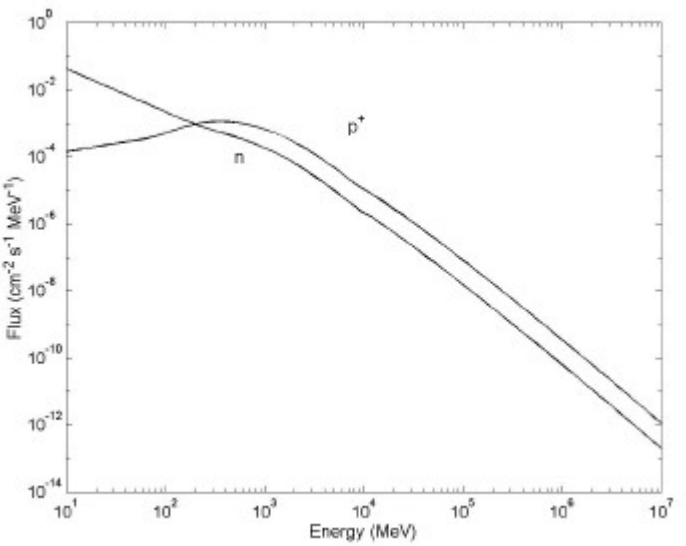

Fig. 13.4 Flux of cosmic ray particles at the present surface of Mars. At present Mars is only protected by its thin 6 mbar CO_2 atmosphere. Most of this radiation reaches the surface. The surface flux compared to the ancient atmospheric conditions is, therefore, several orders of magnitude larger.

13.5 Conclusions

The presence of an ancient strong magnetic field had significant effects on the evolution of the Martian atmosphere – especially on non-thermal escape processes like atmospheric sputtering or solar-wind pick up – and is one of the reasons for the existence of the denser early Martian atmosphere (1 bar or more) 3.7 Ga ago. The escape of water from Mars would also have been reduced by such a magnetic field, an important aspect in the discussion about extinct life on Mars. This ancient thick atmosphere was more effective in shielding the planet from harmful radiation by absorption processes than the magnetic field itself. Only cosmic rays with energy lower than ~10 MeV are significantly affected by the magnetic field, however, a dense early atmosphere is able to absorb most of the cosmic rays and reduced the flux of cosmic ray induced particles by several order of magnitude as compared to the present. The formation of a magnetosphere enabled direct shielding effects able to deflect part of the solar-wind and a Van Allen type radiation belt, which could also trap cosmic ray particles at the lower end of the cosmic ray energy spectrum.

Acknowledgments: The authors would like to thank H. Lichtenegger, Institute for Space Research, Austrian Academy of Sciences, for providing Fig. 13.1.

13.6 References

1 D.M. Hunten, Planet. Space Sci. **30**, 773 (1982).
2 F.L. Walls, G.H. Dunn, J. Geophys. Res. **79**, 1911 (1974).
3 W.B. Hanson, G.P. Mantas, J. Geophys. Res. **93**, 7538 (1988).
4 D.P. Kella, P.J. Johnson, H.B. Pedersen, V. Christensen, L.H. Andersen, Science **276**, 1530 (1997).
5 S. Kumar, D.M. Hunten, A.L. Broadfoot, Planet. Space Sci. **26**, 1063 (1978).
6 S. Kumar, D.M. Hunten, H.A. Taylor, Geophys. Res. Lett **8**, 237 (1981).
7 R.R. Hodges Jr., B.A. Tinsley, J. Geophys. Res. **86**, 7649 (1981).
8 R.R. Hodges Jr., B.A. Tinsley, Icarus **51**, 440 (1982).
9 J.M. Rodriguez, M.J. Prather, M.B. McElroy, Planet. Space Sci. **32**, 1235 (1984).
10 W.-H. Ip, Icarus **76**, 135 (1988).
11 A.F. Nagy, T.E. Cravens, J.-H. Yee, I.F. Stewart, Geophys. Res. Lett. **8**, 629 (1981).
12 J.L. Fox, A. Hac, J. Geophys. Res. **102**, 24,005 (1997).
13 J. Kim, A.F. Nagy, J.L. Fox, T.E. Cravens, J. Geophys. Res. **103**, 29,339 (1998).
14 H. Lammer, S.J. Bauer, Geophys. Res. Lett. **23**, 3353 (1996).
15 J.G. Luhmann, J. Geophys. Res. **102**, 1637 (1997).
16 H. Lammer, S.J. Bauer, J. Geophys. Res. **96**, 1819 (1991).
17 H. Lammer, W. Stumptner, S.J. Bauer, Planet. Space Sci. **48**, 1473 (2000).
18 M.B. McElroy, Science **175**, 443 (1972).
19 R.T. Brinkmann, Science **174**, 944 (1971).
20 J.L. Fox, A. Dalgarno, J. Geophys. Res. **88**, 9027 (1983).
21 E.M. Sieveka, R.E. Johnson, Astrophys. J. **287**, 418 (1984).
22 R.E. Johnson, in: *Energetic Charged-particle Interactions with Atmospheres and Surfaces*, Springer, Berlin, 1990.

23 J.G. Luhmann, R.E. Johnson, M.H.G. Zhang, Geophys. Res. Lett. **19**, 2151 (1992).
24 B.M. Jakosky, R.O. Pepin, R.E. Johnson, J.L. Fox, Icarus **111**, 271 (1994).
25 R. E. Johnson, M. Liu, Science **274**, 1932, 1996.
26 D.M. Kass, Y.L. Yung, Science **274**, 1932 (1996).
27 R.E. Johnson, F. Leblanc, Planet. Space Sci. **49**, 645 (2001).
28 R. Lundin, E.M. Dubinin, Adv. Space Res. **9**, 255 (1992).
29 J. Kar, K.K. Mahajan, R. Kohli, J. Geophs. Res. **101**, 12,747 (1996).
30 A. Miura, P.L. Prichett, J. Geophys. Res. **87**, 7431 (1982).
31 H. Lammer, M.H.G. Zhang, W. Düregger, S.J. Bauer, Internal Report No 86, Austrian Academy of Sciences, 1993.
32 R. Lundin, A. Zakharov, R. Pellinen, S.W. Barabash, H. Borg, E.M. Dubinin, B. Hulquist, H. Koskinen, I. Liede, N. Pissarenko, Geophys. Res. Lett. **17**, 873 (1990).
33 G. Neukum, R. Jaumann, E. Hauber, in *Lecture Notes in Physics*, Springer, Berlin, 2001.
34 M.H. Carr, Nature **326**, 30 (1987).
35 J.C.G. Walker, Icarus **68**, 87 (1986).
36 H.J. Melosh, A.M. Vickery, Nature **338**, 487 (1989).
37 C.F. Chyba, Nature **343**, 129 (1990).
38 G. Kargl, S.J. Bauer, in: *Sitzungsber. Abt. II (1995)*, Austrian Academy of Sciences, Springer, Vienna **131**, 1995, p. 45.
39 K.J. Zahnle, J.C.G. Walker, Rev. Geophys. **20**, 280 (1982).
40 S.C. Liu, T.M. Donahue, Icarus **28**, 231 (1976).
41 T.M. Donahue, Nature **374**, 432 (1995).
42 J. Kar, Geophys. Res. Lett. **17**, 113 (1990).
43 H. Lammer, S.J. Bauer, J. Geophys. Res. **97**, 20,925 (1992).
44 M.H. Acuña, J.E.P. Connerney, P. Wasilewski, R.P. Lin, K.A. Anderson, C.W. Carlson, J. McFadden, D.W. Curtis, D. Mitchell, H. Reme, C. Mazelle, J.A. Sauvaud, C. d`Uston, A. Cros, J.L. Medale, S.J. Bauer, P. Cloutier, M. Meyhew, D. Winterhalter, N.F. Ness, Science **279**, 1676 (1998).
45 J.E.P. Connerney, M.H. Acuña, P.J. Wasilewski, N.F. Ness, H. Rème, C. Mazelle, D. Vignes, R.P. Lin, D.L. Mitchell, P.A. Cloutier, Science **284**, 794 (1999).
46 M. Lewling, T. Spohn, Planet. Space Sci. **45**, 1389 (1997).
47 G. Schubert, T. Spohn, J. Geophys. Res. **95**, 14,095 (1990).
48 D.J. Stevenson, T. Spohn, G. Schubert, Icarus **54**, 466 (1983).
49 K.S. Hutchins, B.M. Jakosky, J. Geophys. Res. **102**, 9183 (1997).
50 D.S. McKay, E.K. Gibson Jr., K.L. Thomas-Keprta, H. Vali, C.S. Romanek, S.J. Clemett, X.D.F. Chiller, C.R. Maechling, R.N. Zare, Science **273**, 924 (1996).
51 D.S. McKay, K.L. Thomas-Keprta, C.S. Romanek, E.K. Gibson Jr., H. Vali, Science **274**, 2123 (1996).
52 J.W. Schopf, in: L.M. Celnikier, J. Trân Thanh Vân (Eds.) *Planetary Systems the long view*, Edition Frontiérs, **463**, 1997.
53 M.V. Zombeck, in: *Handbook of Astronomy and Astrophysics*, Cambridge University Press, 1990.
54 K. O'Brien, in: *REP. EML-338*, Environ. Meas. Lab., New York, 1978.
55 G.J. Molina-Cuberos, J.J. López-Moreno, R. Rodrigo, L.M. Lara, Planet. Space Sci. **47**, 1347 (1999).
56 K.J. Zahnle, J.C.G. Walker, Reviews of Geophys. and Space Phys. **20**, 280 (1982).
57 G.J. Molina-Cuberos, W. Stumptner, H. Lammer, N.I. Kömle, K. O'Brien, Icarus, 2001, in press.